Postzygotic inactivating mutations of *RHOA* cause a mosaic neuroectodermal syndrome

Pierre Vabres[1,2,3,24]*, Arthur Sorlin[1,2,3,4,24], Stanislav S. Kholmanskikh[5,24], Bénédicte Demeer[6], Judith St-Onge[1,2,7], Yannis Duffourd[1,2], Paul Kuentz[1,2,8] Jean-Benoît Courcet[1,2,4], Virginie Carmignac[2,3], Philippine Garret[1,2], Didier Bessis[9], Odile Boute[10], Alain Bron[11], Guillaume Captier[12], Esther Carmi[13], Bernard Devauchelle[14], David Geneviève[15], Catherine Gondry-Jouet[16], Laurent Guibaud[17], Arnaud Lafon[18], Michèle Mathieu-Dramard[6], Julien Thevenon[1,2,4], William B. Dobyns[19], Geneviève Bernard[7,20,21], Satyamaanasa Polubothu[22], Francesca Faravelli[22], Veronica A. Kinsler[22], Christel Thauvin[1,2,4], Laurence Faivre[1,2,4,25], M. Elizabeth Ross[5,25] & Jean-Baptiste Rivière[1,2,7,23,25]*

[1]Fédération Hospitalo-Universitaire Médecine Translationnelle et Anomalies du Développement, CHU Dijon Bourgogne, Dijon, France. [2]UMR Inserm 1231 Génétique des Anomalies du Développement, Université Bourgogne Franche-Comté, Dijon, France. [3]Centre de Référence MAGEC, Service de Dermatologie, CHU Dijon Bourgogne, Dijon, France. [4]Service de Pédiatrie 1 et de Génétique Médicale, CHU Dijon Bourgogne, Dijon, France. [5]Center for Neurogenetics, Feil Family Brain and Mind Research Institute, Weill Cornell Medicine, New York, New York, USA. [6]Unité de Génétique Médicale et Oncogénétique, CHU Amiens Picardie, Amiens, France. [7]Child Health and Human Development Program, Research Institute of the McGill University Health Centre, Montreal, Quebec, Canada. [8]Génétique Biologique Histologie, CHRU de Besançon, Besançon, France. [9]Département de Dermatologie, CHU de Montpellier, Montpellier, France. [10]Service de Génétique Clinique, CHU Lille, Lille, France. [11]Service d'Ophtalmologie, CHU Dijon Bourgogne, Dijon, France. [12]Service de Chirurgie orthopédique et plastique pédiatrique, CHU de Montpellier, Montpellier, France. [13]Dermatology Office, 34 Avenue d'Allemagne, Amiens, France. [14]Département de Chirurgie Maxillo-Faciale et Stomatologie, CHU Amiens Picardie, Amiens, France. [15]Département de Génétique Médicale, Maladies rares et Médecine Personnalisée, CHU de Montpellier, Montpellier, France. [16]Départment de Radiologie, CHU Amiens Picardie, Amiens, France. [17]Service d'Imagerie Pédiatrique et Fœtale, Hôpital Femme-Mère-Enfant Louis Pradel, Hospices Civils de Lyon, Bron, France. [18]Service d'Odontologie-Stomatologie, CHU Dijon Bourgogne, Dijon, France. [19]Center for Integrative Brain Research, Seattle Children's Research Institute, Seattle, Washington, USA. [20]Departments of Neurology and Neurosurgery, and Pediatrics McGill University, Montreal, Quebec, Canada.

30   [21]Department of Medical Genetics, Montreal Children's Hospital, McGill University Health Centre, Montreal,

31   Quebec, Canada. [22]Institute of Child Health, University College London, London, UK. [23]Department of Human

32   Genetics, Faculty of Medicine, McGill University, Montreal, Quebec, Canada. [24]These authors contributed

33   equally to this work. [25]These authors jointly directed this work. *Correspondence should be addressed to P.V.

34   (pierre.vabres@chu-dijon.fr) or J.-B.R. (jean-baptiste.riviere@mcgill.ca).

35

36

37

Hypopigmentation along Blaschko's lines is a hallmark of a poorly defined group of mosaic syndromes whose genetic causes are unknown. Here we show that postzygotic inactivating mutations of *RHOA* cause a neuroectodermal syndrome combining linear hypopigmentation, alopecia, apparently asymptomatic leukoencephalopathy, and facial, ocular, dental, and acral anomalies. Our findings pave the way towards elucidating the etiology of pigmentary mosaicism and highlight the role of *RHOA* in human development and disease.

Linear hypopigmentation, which is commonly seen as a non-specific manifestation of mosaicism, is currently classified using poorly defined umbrella terms such as "pigmentary mosaicism" and "hypomelanosis of Ito"[1]. Because of its frequent association with various extracutaneous anomalies (especially cerebral involvement and epilepsy), hypomelanosis of Ito is often considered as a neurocutaneous syndrome, the fourth most common after neurofibromatosis, tuberous sclerosis complex, and Sturge-Weber syndrome[2]. Apart from rare reports of non-recurrent mosaic chromosomal anomalies[1], the genetic causes of pigmentary mosaicism have remained largely unknown, which hinders diagnosis and patient care.

As part of our research program on mosaic skin disorders, we ascertained seven unrelated individuals with a remarkably similar constellation of features that did not match any known syndrome (**Fig. 1**, **Supplementary Figs. 1** and **2**, and **Supplementary Table 1**). Key clinical features included linear hypopigmentation and hypotrichosis following the lines of Blaschko, symmetric or asymmetric facial dysmorphism (microstomia, malar hypoplasia, downslanting palpebral fissures, and broad nasal bridge), acral anomalies (brachydactyly, syndactyly, and broad first toe), teeth anomalies (oligodontia, microdontia, conical teeth, and abnormal enamel), and ocular anomalies (microphthalmia, strabismus, and myopia). Brain magnetic resonance imaging (MRI) was available for three patients and showed diffuse cystic leukoencephalopathy with mildly enlarged lateral ventricles (**Fig. 1** and **Supplementary Fig. 2**). Despite this striking brain phenotype, no intellectual deficiency or neurological impairment was noted in any affected individual. Linear hypopigmentation following Blaschko's lines, asymmetric craniofacial and brain features, and sporadic occurrence were highly suggestive of mosaicism.

We hypothesized that this previously unrecognized mosaic neuroectodermal syndrome was likely to result from postzygotic mutations in the same gene. We conducted whole-exome sequencing (WES) in two parent–case trios (subjects S1 and S2) using genomic DNA derived from patients' affected skin and parental blood samples (Online Methods and **Supplementary Table 2**). We identified the same postzygotic change of

RHOA (NM_001664.3:c.139G>A; NP_001655.1:p.(Glu47Lys)) supported by 30.6% (44/144) and 2.6% (6/228) of

reads in subjects S1 and S2, respectively (**Supplementary Figs. 3** and **4**, and **Supplementary Table 3**). We

confirmed the presence and postzygotic nature of these mutations by targeted ultra-deep sequencing of the

region spanning the c.139G>A substitution in all available DNA samples from the two patients and their parents

(Methods and **Supplementary Tables 4-6**). Trio-based WES in a third patient (subject S3) led to identification of

another postzygotic *RHOA* change (NM_001664.3:c.211C>T; NP_001655.1:p.(Pro71Ser)) supported by 24.3%

(28/115) of reads (**Supplementary Fig. 5**), thus confirming mutations of *RHOA* as the cause of this novel

syndrome. Amplicon-based ultra-deep sequencing of *RHOA* coding exons in skin-derived DNA from the

remaining three affected individuals, and Sanger sequencing of *RHOA* in one extra individual, led to

identification of the recurrent c.139G>A change (encoding p.Glu47Lys) in three (S4, S5 and S7), for a total of

five patients with the exact same change (**Supplementary Table 6**). This G to A transition occurs at a CpG

dinucleotide, which might at least partly explain its recurrence. Subject S6 could not be analyzed due to failed

quality controls. Both *RHOA* mutations (c.139G>A and c.211C>T) were absent from dbSNP (build 147,

https://www.ncbi.nlm.nih.gov/snp/), major public variant databases, and in-house WES data from ~1,500

individuals. They affect highly conserved nucleotides and amino acids, and are predicted as pathogenic *in silico*

(**Supplementary Table 7**). All mutations were absent from blood samples of affected individuals. In skin-derived

DNA samples, mutant allele fractions ranged from 1.9% to 33.5% with higher levels in fresh skin than in cultured

skin fibroblasts (**Fig. 1j** and **Supplementary Table 6**), possibly due to negative selection of mutant cells during

cell culture. WES in S2 also revealed a previously unknown familial NC_012920.1:m.11778G>A MT-ND4 in

mitochondrial Complex I mtDNA, causing Leber's hereditary optic neuropathy, and probably responsible for a

more severe loss of visual acuity (**Supplementary Fig. 6**). No *RHOA* mutations were found in 24 additional

subjects with linear hypopigmentation associated with various extracutaneous features (**Supplementary Table 8**).

      RHOA encodes a RAS-related Rho GTPase known to control a wide range of biological functions such

as morphogenesis, chemotaxis, axonal guidance, and cell cycle progression[3]. RhoA has been extensively

studied for its central role in signal transduction and actin cytoskeleton dynamics, through regulation of stress

fibers and focal adhesion formation[4]. The two mutations identified here (encoding p.(Glu47Lys) and p.(Pro71Ser))

are located just downstream of each of the two switch regions (**Fig. 1k**), whose GTP-dependent conformational

changes regulate selective interaction of RhoA with downstream effectors[5]. To assess the impact of the

p.(Glu47Lys) and p.(Pro71Ser) missense changes identified in four of our patients, we compared their effects

98   with two well-characterized *RHOA* mutants, namely dominant-negative p.(Thr19Asn)[6] and constitutively active

99   p.(Gly14Val)[7] changes. We transfected NIH3T3 cells with FLAG-tagged mutants and wild-type *RHOA* plasmids.

100   Immunocytochemical labeling of F-actin stress fibers and microtubules revealed marked cytoskeletal alterations

101   in cells transfected with both mutant plasmids. Similar to the *RHOA* dominant-negative p.(Thr19Asn) mutant,

102   p.(Glu47Lys) and p.(Pro71Ser) expressing cells displayed reduced cell spreading and decreased number of

103   stress fibers, as well as microtubule disorganization (**Fig. 2a,b**), thus indicating a dominant-negative or otherwise

104   inactivating effect for these two mutations. Consistent with these findings, Western blot analysis of NIH3T3 cells

105   transfected with the dominant-negative p.(Thr19Asn), p.(Glu47Lys) RhoA, or p.(Pro71Ser) RhoA revealed

106   reduced levels of endogenous myosin phosphatase target subunit 1 (MYPT1) phosphorylated at Thr696, and

107   myosin light chain 2 (MLC2) phosphorylated at Thr19, both sites targeted by Rho kinase 1 (ROCK1), a major

108   downstream effector of activated RhoA[8] (**Fig. 2c** and **Supplementary Fig. 7**).

109   We have delineated a clinical and molecular subset of pigmentary mosaicism, which we propose to

110   name "*RHOA*-related mosaic ectodermal dysplasia". Apart from recent reports of linear hypopigmentation in six

111   patients with *MTOR*-related hemimegalencephaly[9], no specific genes have been implicated in pigmentary

112   mosaic disorders. Our findings highlight the value of careful clinical phenotyping combined with massively

113   parallel sequencing for elucidating their genetic causes. The syndrome described here presents both similarities

114   and notable differences with other mosaic syndromes involving the skin, such as disorders of the PI3K-AKT-

115   mTOR and RAS-MAPK pathways[10]. RhoA is a highly conserved protein particularly intolerant to amino acid

116   substitutions, with only five observed missense changes in the Exome Aggregation Consortium (66.9 expected

117   variants; z = 3.70) and no loss-of-function alleles (5.1 expected)[11]. Accordingly, *RHOA* is part of the "core

118   essentialome", a set of genes essential to cell viability[12,13], thus supporting the idea that *RHOA*-related mosaic

119   ectodermal dysplasia should be added to the list of disorders resulting from lethal mutations surviving only by

120   mosaicism, which includes Proteus, Sturge-Weber, and some other mosaic syndromes[14]. All postzygotic

121   mutations reported to date as causing such mosaic syndromes have been activating mutations also frequently

122   found in somatic cancer[15]. Our data show that disease-causing lethal mutations surviving by mosaicism can act

123   through a likely dominant-negative effect. Intriguingly, although both dominant-negative and activating *RHOA*

124   mutations are known somatic driver mutations in several cancer types, neither of the two mutations identified

125   here has been reported in cancer (**Supplementary Table 9**). The absence of both variants in blood, as

126   commonly observed in mosaic development disorders[16], is consistent with the known pivotal role of RhoA in

127   hematopoietic stem cell and lymphocyte development[17], suggesting negative selection of mutant blood cells.

5

128   Hence, for diagnostic purpose, mutation testing in *RHOA*-related mosaic ectodermal dysplasia should be

129   performed on a biopsy from affected skin, as in other mosaic conditions. We hypothesize that most clinical

130   manifestations in *RHOA*-related mosaic ectodermal dysplasia result from anomalies in cell migration, particularly

131   in the brain and eye. However, we cannot exclude additional mechanisms, such as inhibition of NFκB, or

132   alteration of the Wnt pathway, similar to male-lethal X-linked diseases incontinentia pigmenti or focal dermal

133   hypoplasia, since RhoA is involved in the regulation of both pathways[18–20], Finally, similar to mosaic overgrowth

134   disorders of the PI3K-AKT-mTOR pathway, identification of other genes causing ectodermal mosaic syndromes

135   may pinpoint common pathogenesis pathways, which will help enhancing our understanding of their causes, and

136   ultimately result in novel therapeutic opportunities.

137

138

147

148   **AUTHOR CONTRIBUTIONS**

149   P.V. and J.-B.R. designed the study. A.S., J.S.-O., P.K., J.-B.C., V.C., S.P. and V.A.K. performed the genetics

150   experiments. J.-B.R., Y.D. and P.G. performed the bioinformatics experiments. S.S.K. performed the functional

151   experiments. P.V., A.S., B. Demeer, D.B., O.B., A.B., G.C., E.C., C.T., S.P., F.F., V.A.K., B. Devauchelle, D.G.,

152   C.G.-J., A.L., M.M.-D., J.T. and L.F. recruited and evaluated the study subjects. L.G., G.B. and W.B.D. analyzed

153   the brain MRI. P.V., L.F., M.E.R. and J.-B.R. supervised the study. P.V., A.S., S.S.K, M.E.R. and J.-B.R. wrote

154   the manuscript. All authors revised the manuscript.

155

156   **COMPETING FINANCIAL INTERESTS**

157   The authors declare no competing financial interests.

FIGURES

159 **Figure 1 | Main clinical features of *RHOA*-related mosaic ectodermal dysplasia and *RHOA* mutations. a-e**,

160 Craniofacial appearance, linear hypopigmentation and other extracutaneous anomalies in subject S1. **f-i**, Brain

161 MRI of subject S1 at 15 years. A second MRI, conducted 6 months later, did not show any significant change.

162 Subjects S2 and S4 had similar but milder MRI abnormalities, including enlarged temporal horns of the lateral

163 ventricles (**Supplementary Fig. 2**). Sagittal T1-weighted image revealed preserved midline structures (**f**). Axial

164 T2-weighted images revealed a focal hyperintense lesion in the right hemisphere of the cerebellum (**g**,

165 arrowhead), and diffuse cystic leukoencephalopathy with mildly enlarged lateral ventricles and cysts in the

166 thalami and caudate nuclei (**h**). The leukoencephalopathy and presence of multiple cysts is confirmed on fluid-

167 attenuated inversion recovery (FLAIR) sequences (**i**). **j**, Mutant allele fraction of *RHOA* mutations in the five

168 subjects studied in WES or TUDS. **k**, Linear representation of *RHOA* and localization of the two mutations.

169

170 **Figure 2 | Inactivating effect of the two *RHOA* mutations. a,b**, Cytoskeletal organization and morphology in

171 NIH/3T3 cells transfected with wild-type, constitutively active (p.Gly14Val), dominant-negative (p.Thr19Asn),

172 (p.Glu47Lys) and (p.Pro71Ser) forms of *RHOA*. **a**, Up: Cells transfected with wild-type *RHOA* or p.Gly14Val

173 mutant display expected increase in F-actin staining, particularly with regard to stress fibers which are brighter,

174 thicker and more numerous. Cells transfected with p.Thr19Asn, p.Glu47Lys or (p.Pro71Ser) mutants barely

175 contain any stress fibers at all. Low: Dual labeling for DAPI (blue) and alpha-tubulin (green) does not reveal

176 significant differences in the gross organization of microtubule cytoskeleton or nuclear morphology between

177 different mutants. All cells (n = 20 per group) selected at random across the cover slip that were individually

178 examined showed reduced stress fibers and limited cell spreading. **b**, Up: FLAG staining does not reveal any

179 visible differences in the subcellular localization of different RhoA mutants. All mutants tend to impair cell

180 spreading, while wild-type RhoA overexpressing cells maintain normal morphology. Middle: Dual labeling for

181 DAPI (blue) and pMYPT1 (red) shows decrease in signal intensity of MYPT1(pT696) staining upon transfection

182 with T19N (control), E47K or P71S mutants. Low: Quantification of MYPT1(pThr696) staining shows significant

183 decrease (n = 20, 24, 14, 30, and 13 cells, for WT, G14V, T19N, E47K, and P71S, respectively). Box plot

184 elements: 5°, 25°, median, mean (cross), 75° and 95°percentiles. **c**, Levels of phosphorylated MYPT1(pThr696)

185 and MLC2(pThr19). Left: Cropped images of Western blot experiment showing expression levels of total MYPT1,

186 phospho-MYPT1, total MLC2, and phospho-MLC2. There is a visible reduction in phospho-MYPT1 and

187 phospho-MLC2 when RhoA(Thr19Asn) or RhoA(Glu47Lys) are overexpressed. Middle and right: dot plot of

188 normalized ratio (4 independent experiments) for phospho-MYPT1 and phospho-MLC2 normalized to total

189 MYPT1 and MLC2, respectively, indicate reduction in MYPT1(pThr696) and MLC2(pThr19) upon

190 RhoA(Glu47Lys) or RhoA(Pro71Ser) overexpression. Further analyses for p.(Glu47Lys) are shown in

191 **Supplementary Figure 7**. Full scans of blots are provided in **Supplementary Figure 8**.

192

193 **REFERENCES**

194

195 1.   Sybert, V. P. Hypomelanosis of Ito: a description, not a diagnosis. *J. Invest. Dermatol.* **103**, S141–S143
196 (1994).
197 2.   Pavone, P., Praticò, A. D., Ruggieri, M. & Falsaperla, R. Hypomelanosis of Ito: a round on the frequency
198 and type of epileptic complications. *Neurol. Sci.* **36**, 1173–1180 (2015).
199 3.   Canman, J. C. *et al.* Inhibition of Rac by the GAP activity of Centralspindlin is essential for cytokinesis.
200 *Science* **322**, 1543–1546 (2008).
201 4.   Hall, A. Rho GTPases and the actin cytoskeleton. *Science* **279**, 509–514 (1998).
202 5.   Vetter, I. R. & Wittinghofer, A. The guanine nucleotide-binding switch in three dimensions. *Science* **294**,
203 1299–1304 (2001).
204 6.   Pan, Z. K. *et al.* Role of the Rho GTPase in bradykinin-stimulated nuclear factor-κB activation and IL-1β
205 gene expression in cultured human epithelial cells. *J. Immunol.* **160**, 3038–3045 (1998).
206 7.   Zhao, X. *et al.* Overexpression of RhoA induces preneoplastic transformation of primary mammary
207 epithelial cells. *Cancer Res.* **69**, 483–491 (2009).
208 8.   Maekawa, M. *et al.* Signaling from Rho to the actin cytoskeleton through protein kinases ROCK and LIM-
209 kinase. *Science* **285**, 895–898 (1999).
210 9.   Mirzaa, G. M. *et al.* Association of MTOR mutations with developmental brain disorders, including
211 megalencephaly, focal cortical dysplasia, and pigmentary mosaicism. *JAMA Neurol.* **73**, 836–845 (2016).
212 10.   van Steensel, M. A. M. Neurocutaneous manifestations of genetic mosaicism. *J. Pediatr. Genet.* **4**, 144–
213 153 (2015).
214 11.   Lek, M. *et al.* Analysis of protein-coding genetic variation in 60,706 humans. *Nature* **536**, 285–291
215 (2016).
216 12.   Blomen, V. A. *et al.* Gene essentiality and synthetic lethality in haploid human cells. *Science* **350**, 1092–
217 1096 (2015).
218 13.   Wang, T. *et al.* Identification and characterization of essential genes in the human genome. *Science* **350**,
219 1096–1101 (2015).
220 14.   Happle, R. Cutaneous manifestation of lethal genes. *Hum. Genet.* **72**, 280 (1986).
221 15.   Fernández, L. C., Torres, M. & Real, F. X. Somatic mosaicism: on the road to cancer. *Nat. Rev. Cancer*
222 **16**, 43–55 (2016).
223 16.   Kuentz, P. *et al.* Molecular diagnosis of PIK3CA-related overgrowth spectrum (PROS) in 162 patients
224 and recommendations for genetic testing. *Genet. Med.* **19**, 989–997 (2017).
225 17.   Zhang, S., Zhou, X., Lang, R. A. & Guo, F. RhoA of the Rho family small GTPases is essential for B
226 lymphocyte development. *PLoS ONE* **7**, e33773 (2012).
227 18.   Tong, L. & Tergaonkar, V. Rho protein GTPases and their interactions with NFκB: crossroads of
228 inflammation and matrix biology. *Biosci. Rep.* **34**, (2014).
229 19.   Ordóñez-Morán, P. *et al.* RhoA–ROCK and p38MAPK-MSK1 mediate vitamin D effects on gene
230 expression, phenotype, and Wnt pathway in colon cancer cells. *J. Cell Biol.* **183**, 697–710 (2008).
231 20.   Rodrigues, P. *et al.* RHOA inactivation enhances Wnt signalling and promotes colorectal cancer. *Nat.*
232 *Commun.* **5**, 5458 (2014).
233

234

235 **ONLINE METHODS**

236 **Study subjects.** The study included seven unrelated affected individuals and their unaffected parents.

237 Individuals were phenotyped and recruited by geneticists and dermatologists in Dijon and elsewhere in France

238 through a collaborative nationwide effort to identify genes causing mosaic syndromes involving the skin

239 (ClinicalTrial registration number NCT01950975, https://clinicaltrials.gov/). Inclusion criteria consisted of the

240 following: sporadic condition, congenital or early childhood onset, and cutaneous lesions with a pattern

241 suggestive of mosaicism associated with extracutaneous anomalies. We obtained written informed consent from

242 all subjects or their legal representatives, and the ethics committee of Dijon University Hospital approved the

243 study. We extracted genomic DNA from fresh skin, cultured skin fibroblasts, and blood samples using the Gentra

244 Puregene Blood and Tissue Extraction Kit (Qiagen). We assessed genomic DNA integrity and quantity by

245 agarose gel electrophoresis, NanoDrop spectrophotometry, and Qubit fluorometry (Thermo Fisher).

246

247 **Whole-exome sequencing (WES).** Exome capture and sequencing were performed at Integragen (Evry,

248 France) from 1 μg of genomic DNA per individual using the Agilent SureSelect Human All Exon V5 (trios S1 and

249 S2) and Clinical Research Exome (trio S3) kits. Libraries were sequenced on a HiSeq platform (Illumina) using

250 paired-end 75-bp reads. Sequences were aligned to the human genome reference sequence (GRCh37/hg19

251 build of UCSC Genome Browser), and single-nucleotide variants and small insertions/deletions were

252 systematically detected as previously described[21]. Candidate *de novo* mutational events were identified by

253 focusing on protein-altering and splice-site changes: (i) supported by at least three reads and 10% of total reads

254 in the proband; (ii) absent in both parents, as defined by variant reads representing less than 5% of total reads;

255 (iii) at base-pair positions covered by at least four reads in the entire trio; and (iv) present at a frequency less

256 than 1% in dbSNP (build 147) and 0.1% in the Exome Aggregation Consortium (ExAC,

257 http://exac.broadinstitute.org/)[11]. Candidate low-level postzygotic changes of *RHOA* in subject S2 were detected

258 as previously described[22]. Briefly, all coding and splice-site bases of *RHOA* were systematically analyzed to

259 count all sites with at least one read not matching the reference sequence, using a base-quality threshold of 30.

260

261 **Ultra-deep sequencing of *RHOA*.** Coding exons of *RHOA* (reference accession NM_001664.2) were amplified

262 using custom intronic primers (**Supplementary Table 4**) and standard PCR with the PrimeSTAR GXL DNA

263 Polymerase (Takara Bio). PCR products were purified and libraries were prepared using the transposase-based

9

264 Nextera XT DNA Sample Preparation kit (Illumina). Libraries were sequenced on a MiSeq instrument using 300-

265 cycle reagent kits v2 (Illumina) and paired-end sequencing reactions of 150-bp reads. Ultra-deep sequencing

266 was performed to achieve a sequencing depth of at least 1,000 reads for all targeted coding bases and splice

267 junctions (**Supplementary Table 5**). As previously described[22], we identified candidate single-nucleotide

268 variants and small insertions/deletions by recording all sites of *RHOA* coding exons and splice junctions with at

269 least four reads not matching the reference sequence, using a base quality threshold of 30 and a mapping

270 quality threshold of 20, with a mutant allele fraction of at least 0.01. We annotated variants with SeattleSeq

271 Annotation (http://snp.gs.washington.edu/SeattleSeqAnnotation138/), and focused on protein-altering and splice-

272 site changes present at a frequency less than 0.1% in ExAC[11].

273

274 ***In silico* prediction.** Nucleotide-level conservation and impact of amino acid change of *RHOA* mutations were

275 assessed using the Genomic Evolutionary Rate Profiling (GERP)[23] and Combined Annotation-Dependent

276 Depletion (CADD) scores[24], respectively (**Supplementary Table 7**).

277

278 **Cell culture and transfection.** NIH/3T3 cells were obtained from ATCC (CRL-1658TM) and maintained in

279 Dulbecco's Modified Eagle's Medium (DMEM (Life Technologies)) plus 10% calf serum. 60% confluent cultures

280 were transfected using XfectTM reagent (Clontech) as per manufacturer's protocol and cultured for 48 hours

281 before lysis or fixation.

282

283 **FLAG-tagged DNA constructs and mutagenesis.** DNA constructs for mammalian expression, including FLAG-

284 tagged wild-type, G14V and T19N mutant RhoA, were obtained from the Missouri S&T cDNA Resource Center

285 (www.cdna.org). E47K and P71S mutations were introduced into the wild-type *RHOA* sequence using the

286 QuickChange site-directed mutagenesis kit (Agilent Technologies), as per manufacturer's protocol along with the

287 primers described in **Supplementary Table 10**. The wild-type or mutant *RHOA* ORFs were then moved to

288 pCMV-Tag2B mammalian expression vector (Stratagene) using standard cloning procedures to create proteins

289 with FLAG tag at the N-terminus.

290

291 **Immunocytochemistry.** NIH/3T3 cells were fixed with 0.25% glutaraldehyde and permeabilized with 0.1%

292 Triton x100 (Sigma). Mouse anti-α-tubulin (T6074, Sigma, 1:5,000) and goat anti-FLAG (A190-101A, Bethyl

10

Laboratories, 1:500) antibodies were incubated overnight at 4 °C. Appropriate secondary AlexaFluor-conjugated antibodies (Life Technologies, 1:1,000) along with AlexaFluor-conjugated phalloidin to visualize F-actin (A12379, Life Technologies, 1:100) were applied for 1 hour at room temperature. Cover glasses were mounted in ProLong anti-fade media (Life Technologies) and visualized with 100x oil objective on inverted microscope (Zeiss) fitted with spinning disc confocal scanner (Perkin-Elmer). Imaging analysis was performed using ImageJ software as follows: Confocal stacks were projected into a single plane (Z-project, Maximal Intensity), images were thresholded and fluorescence intensity measured as a mean gray value. The investigator collecting images was blinded to the experimental groups. During analysis of immunocytochemistry data, the investigator was blinded to the identity of the experimental groups.

Western blotting. NIH/3T3 cells were rinsed once with PBS and lysed in M-PER lysis buffer (Thermo Fisher) supplemented with protease and phosphatase inhibitor cocktail (Sigma). Protein concentration of the lysates cleared of insoluble cell debris were determined using 660 nm Protein Assay reagent (Thermo Fisher). A total of 15 μg of proteins in LDS electrophoresis loading buffer (Life Technologies) was denatured for 10 min at 70 °C and separated on 4-12% SDS-PAGE gel (Life Technologies). Proteins were transferred onto 0.2-μm nitrocellulose membrane (Pall) and processed for Western blotting. Primary antibodies were used at the following dilutions: goat anti-actin (sc-1616, Santa-Cruz Biotechnology, 1:4,000), mouse anti-MYPT1 (612165, Becton-Dickinson, 1:4,000), rabbit anti-MYPT1(pT696) (ABS45, Millipore, 1:500), rabbit anti-RhoA (67B9, Cell Signaling, 1:4,000), rabbit anti-MLC2 (8505, Cell Signaling, 1:4,000), and mouse anti-MLC2(pT19) (3674, Cell Signaling, 1:500). Appropriate secondary IRDye-conjugated antibodies (LI-COR) were used at 1:10,000. Proteins were detected using Odyssey imager (LI-COR). The investigator carrying out the Western blot experiments was not blinded to the identity of the samples.

Myc-tagged DNA constructs and mutagenesis. DNA constructs of myc-tagged wild-type, p.Gly14Val, and p.Thr19Asn RhoA for mammalian expression were obtained from Missouri S&T cDNA Resource Center (www.cdna.org). The c.139G>A mutation (encoding p.Glu47Lys) was introduced into the wild-type *RHOA* sequence using the QuickChange site-directed mutagenesis kit (Agilent Technologies) as per manufacturer's protocol, and primers listed in **Supplementary Table 10**. Other steps were performed as described above, with anti-Myc antibodies instead of anti-FLAG (Bethyl Laboratories, 1:500).

322

Statistics. For fluorescence intensity quantification, a t-test assuming unequal variance was performed, with P-values less than 0.05 considered significant difference. For Western blotting, four independent experiments for each transfection were performed, and average and standard deviation reflect these replicates.

326

Data availability. The data that support the findings of this study are available from the corresponding authors upon reasonable request.

329

Reporting summary. Comprehensive information on experimental design and reagents can be found online in the **Life Sciences Reporting Summary**.

332

Methods-only References

21.   Thevenon, J. *et al.* Diagnostic odyssey in severe neurodevelopmental disorders: toward clinical whole-exome sequencing as a first-line diagnostic test. *Clin. Genet.* **89**, 700–707 (2016).
22.   Rivière, J.-B. *et al. De novo* germline and postzygotic mutations in *AKT3, PIK3R2* and *PIK3CA* cause a spectrum of related megalencephaly syndromes. *Nat. Genet.* **44**, 934–940 (2012).
23.   Cooper, G. M. *et al.* Single-nucleotide evolutionary constraint scores highlight disease-causing mutations. *Nat. Methods* **7**, 250–251 (2010).
24.   Kircher, M. *et al.* A general framework for estimating the relative pathogenicity of human genetic variants. *Nat. Genet.* **46**, 310–315 (2014).
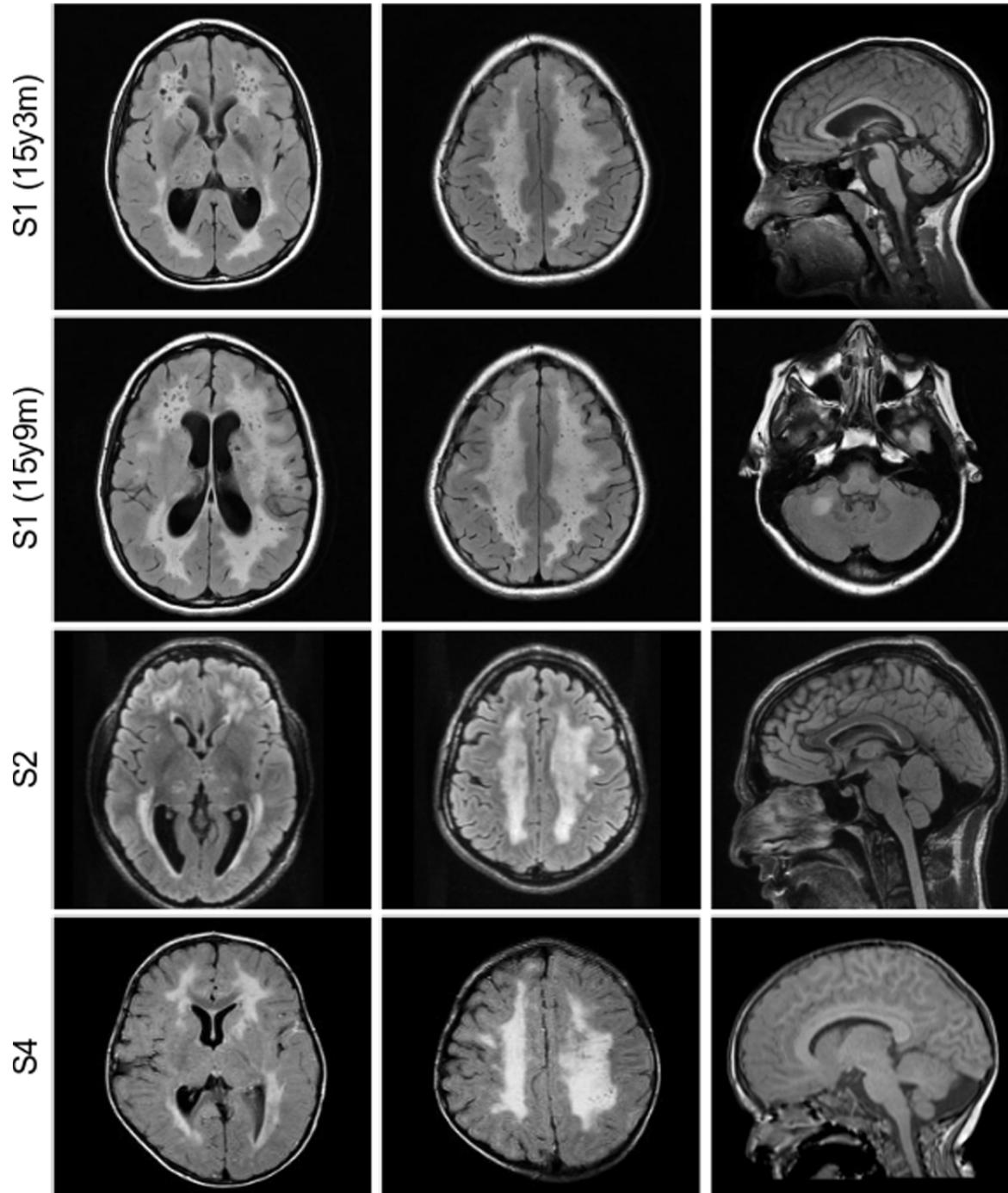
Editorial summary:

Postzygotic inactivating mutations in *RHOA* cause a mosaic neuroectodermal syndrome characterized by linear hypopigmentation, leukoencephalopathy, and craniofacial anomalies, highlighting the role of RHOA in human development and disease.

Supplementary Figure 1

Main clinical features of affected individuals.

a, Craniofacial appearance of affected individuals showing hemifacial microsomia in all subjects. **b**, Patchy alopecia of hair and beard. **c**, Teeth anomalies consisting of oligodontia, microdontia, and conical teeth. **d**, Variable degrees of acral anomalies including symmetric or asymmetric brachydactyly, syndactyly, and polydactyly. Photograph of subject S3 was taken after surgery. **e**, Linear hypopigmentation following Blaschko's lines on trunk, limbs, and face. See **Supplementary Table 1** for additional details. We obtained written consent to publish photographs of these individuals.
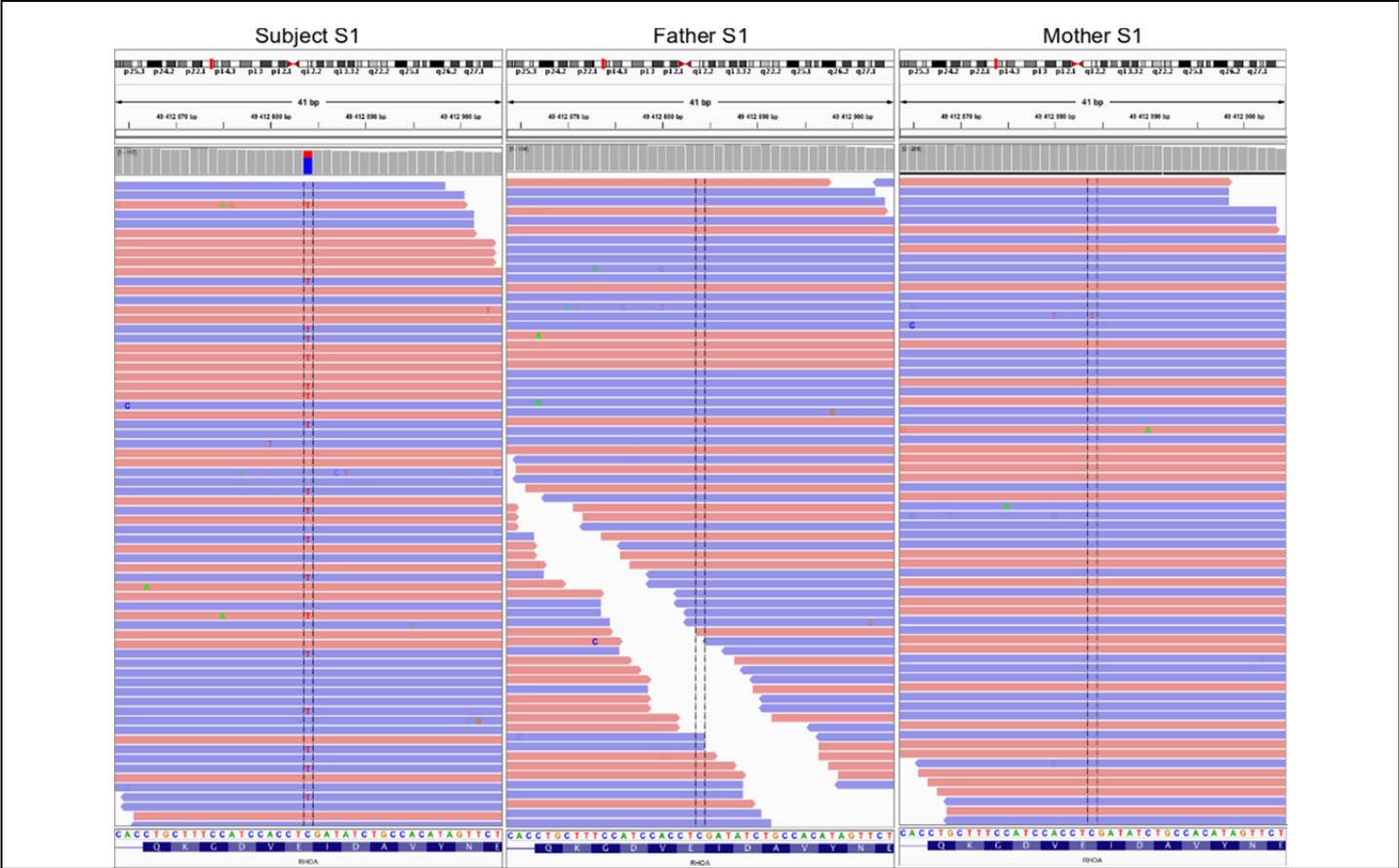
Supplementary Figure 2

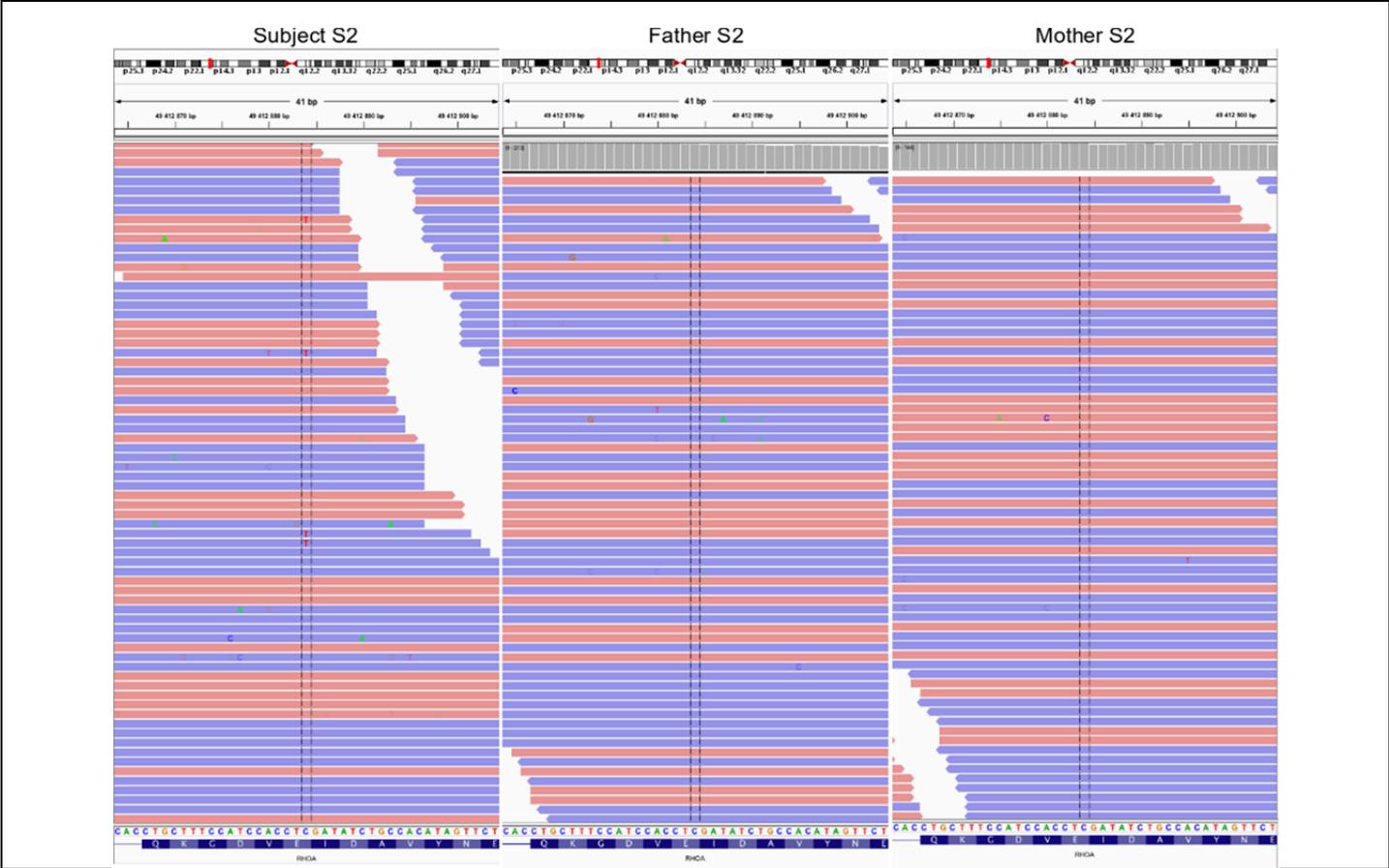**Brain magnetic resonance imaging (MRI) for subjects S1, S2 and S4.**

Brain magnetic resonance imaging (MRI) for subjects S1 (at 15 years and 3 months (first row) and six months later (second row)), S2 (third row), and S4 (fourth row). MRI revealed bilateral and symmetrical marked and diffuse hyperintensities on FLAIR images, with sparing of the subcortical white matter/U-fibers. White matter signal abnormalities extend to the anterior limb of the internal capsule, with sparing of the posterior limb of the capsule, associated with either cystic formation (S1) or relative dilatation of the Virchow-Robin spaces (S1, S2, and S4). Note that the corpus callosum is

spared. No significant anomalies of thalami and infratentorial cerebellar matter were noted in patients S2 and S4. A posterior fossa cyst is observed in 2 out of 3 patients (S2 and S4), with minimal mass effect on the cerebellum. One focal lesion of the cerebellar white matter was noticed in S1, with a hyperintensity on T2 weighted images. Lesions were stable on the 6-months follow-up MRI for subject S1. It is of interest to note that a leukoencephalopathy with enlarged Virchow-Robin spaces has been described in patients with mutations of *PTEN* (Vanderver, A. *et al. Am. J. Med. Genet. A.* **164A,** 627–633 (2014)), a gene that encodes an inhibitor of the PI3K-AKT-mTOR signaling pathway and is known to be regulated by *RHOA* (Li, Z. *et al. Nat. Cell Biol.* **7,** 399–404 (2005)).
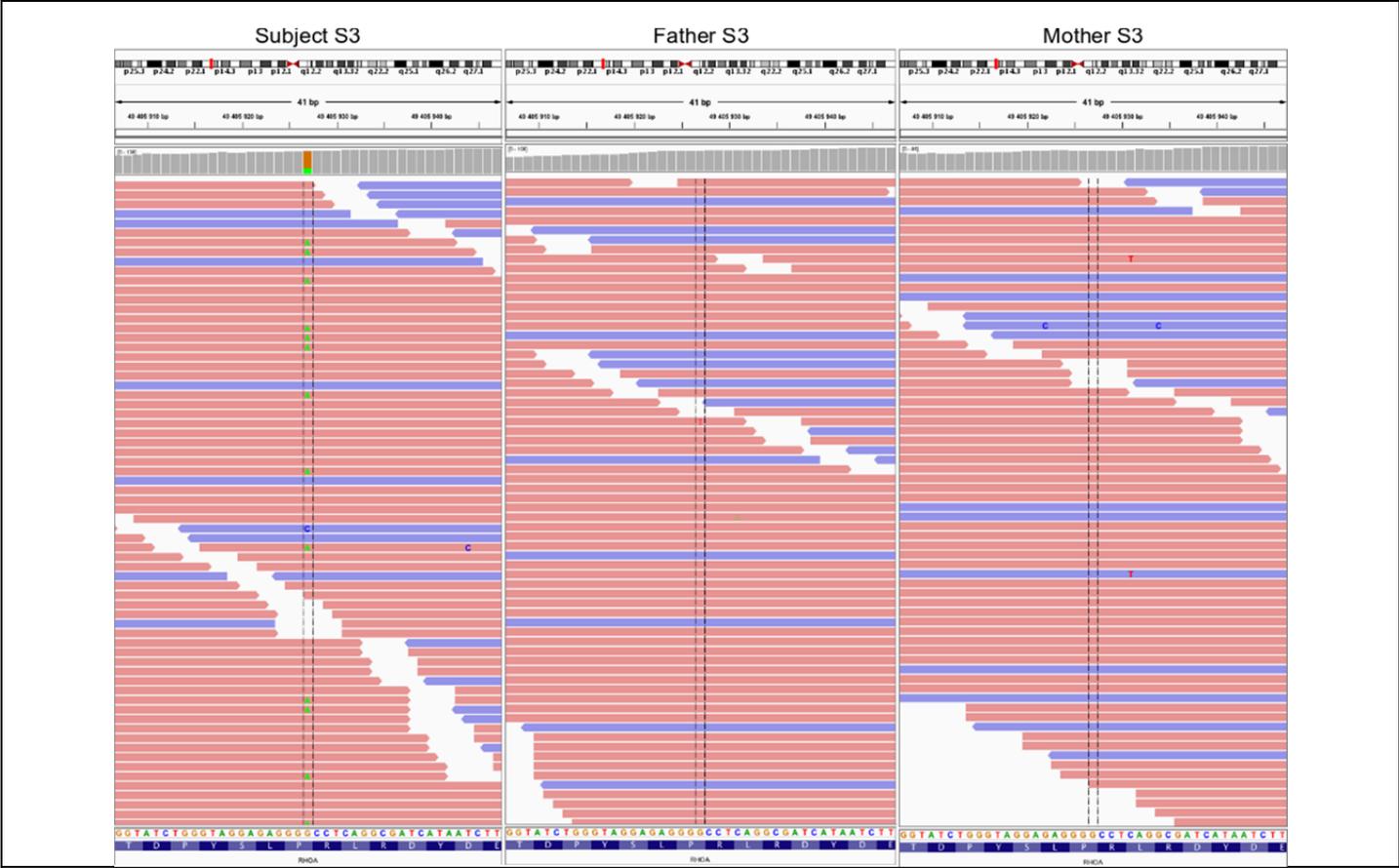
Supplementary Figure 3

Integrative Gemomics Viewer (IGV) screenshots of the *de novo* postzygotic *RHOA* c.139G>A substitution (encoding p.(Glu47Lys)) in subject S1 and her parents.

Supplementary Figure 4

IGV screenshots of the *de novo* postzygotic *RHOA* c.139G>A substitution (encoding p.(Glu47Lys)) in subject S2 and his parents.
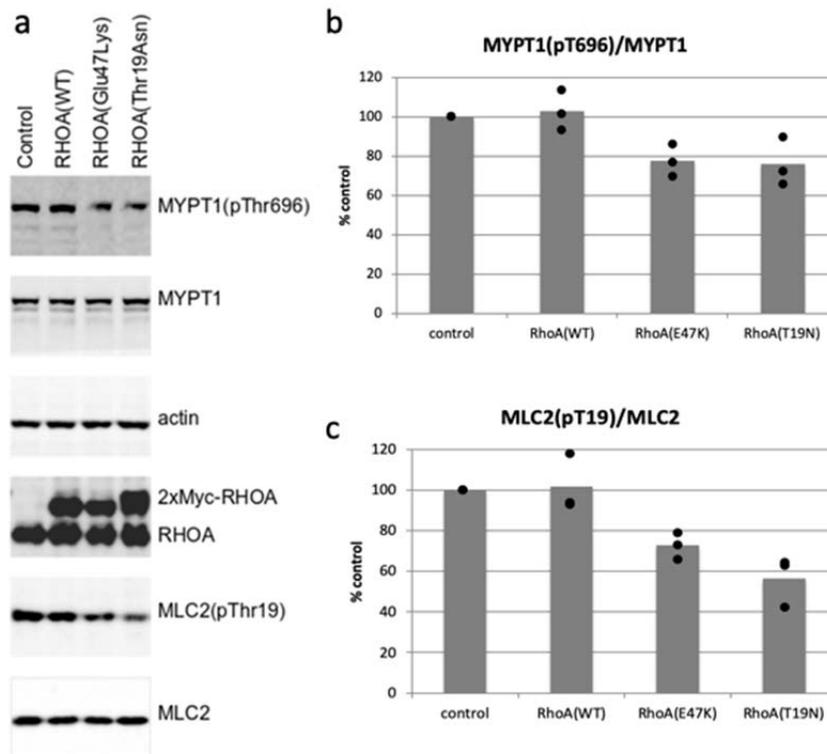
Supplementary Figure 5

IGV screenshots of the *de novo* postzygotic *RHOA* c.211C>T substitution (encoding p.(Pro71Ser)) in subject S3 and her parents.
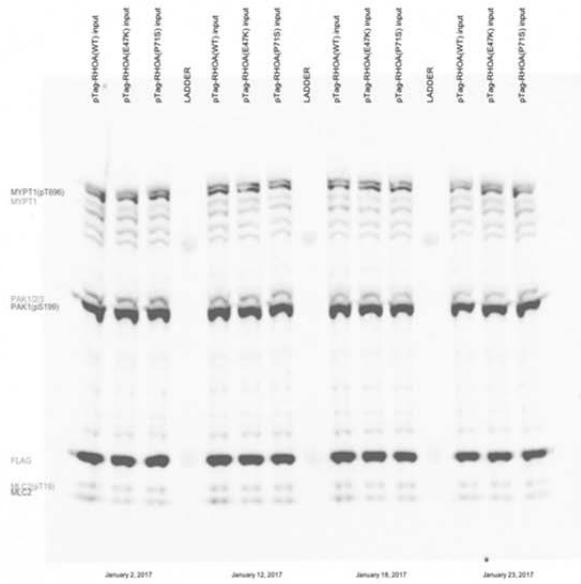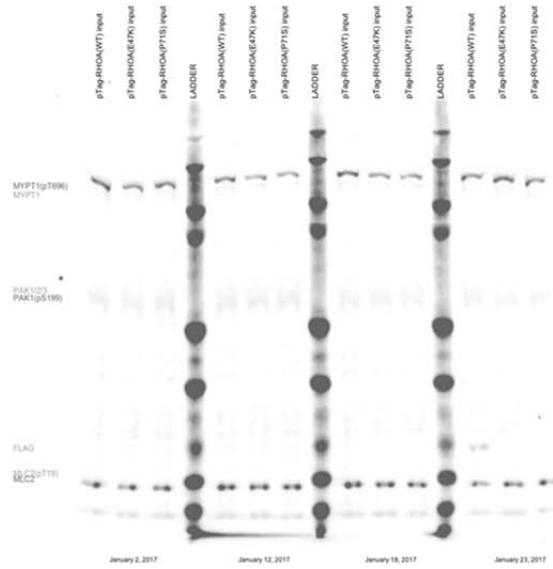
Supplementary Figure 6

IGV screenshots of the NC_012920.1:m.11778G>A, MT-ND4 c.1019G>A, p.(R340H) substitution in S2 (left) and his mother (right).

Supplementary Figure 7

Expression levels of overexpressed wild-type or mutant myc-tagged RhoA, and endogenous RhoA, total MYPT1, phospho-MYPT1 (pThr696), total MLC2, actin, and phospho-MLC2 (pThr19).

a, Representative Western blots show similar protein loading (endogenous total MYPT1, actin, endogenous RhoA, and total MLC2) and similar overexpression of myc-tagged wild-type and mutant RhoA (three independent experiments). There is a visible reduction in phosphorylated MYPT1(pThr696) and MLC2(pThr19) when RhoA(Thr19Asn) or RhoA(Glu47Lys) are overexpressed. **b,c**, Levels of phosphorylated MYPT1(pThr696) and MLC2(pThr19) in endogenous and transfected NIH/3T3 cells. Cumulative data of average density values (overlaid with dots from the three independent experiments) for phosphorylated MLC2(pThr19) (**b**) and MYPT1(pThr696) (**c**) normalized to total MLC2 and MYPT1, respectively, indicate reduction in MLC2(pThr19) and MYPT1(pThr696) upon RhoA(Thr19Asn) or RhoA(Glu47Lys) overexpression.

Supplementary Figure 8

Full scans of blot used in Figure 2.

1

a b c d e f g h i j k

p.Glu47Lys   p.Pro71Ser

G1   G2   G3   G4   G5

Switch 1   Switch 1   Insert region

G motif
Switch
Insert region

Mutant allele fraction
Subject

Blood
Fresh skin
Cultured skin fibroblasts

a

pTAG-RHOA(WT) | pTAG-RHOA(Glu14Val) | pTAG-RHOA(Thr19Asp) | pTAG-RHOA(Glu47Lys) | pTAG-RHOA(Pro71Ser)

Tubulin
FLAG
10μm

DAPI
F-actin

b

pTAG-RHOA(WT) | pTAG-RHOA(Glu14Val) | pTAG-RHOA(Thr19Asp) | pTAG-RHOA(Glu47Lys) | pTAG-RHOA(Pro71Ser)

DAPI
FLAG
10μm

DAPI
MYPT1(pT696)

RHOA(WT) | RHOA(Glu14Val) | RHOA(Thr19Asp) | RHOA(Glu47Lys) | RHOA(Pro71Ser)

c

size marker (kDa) | pTag-RHOA(WT) | pTag-RHOA(E47K) | pTag-RHOA(P71S)

20 / 15 — MLC2(pT18)

20 / 15 — MLC2

150 / 100 — MYPT1(pT696)

150 / 100 — MYPT1

MYPT1(pT696)/MYPT1

Normalized ratio to WT (AU)

WT | RHOA(Glu47Lys) | RHOA(Pro71Ser)

MLC2(pT19)/MLC2

Normalized ratio to WT (AU)

WT | RHOA(Glu47Lys) | RHOA(Pro71Ser)